Reversed polarized emission in highly strained *a*-plane GaN/AlN multiple quantum wells

R. Mata,[1] A. Cros,[1] J. A. Budagosky,[1] A. Molina-Sánchez,[1] N. Garro,[1] A. García-Cristóbal,[1] J. Renard,[2] S. Founta,[2] B. Gayral,[2] E. Bellet-Amalric,[2] C. Bougerol,[2] and B. Daudin[2]

[1]*Materials Science Institute, University of Valencia, P.O. Box 22085, E46071 Valencia, Spain*

[2]*CEA-CNRS Group, Nanophysique et Semiconducteurs, Institut Néel, INAC, SP2M, CNRS-Université Joseph Fourier and CEA Grenoble, 17 rue des Martyrs, 38 054 Grenoble, France*

(Received 23 March 2010; revised manuscript received 22 July 2010; published 3 September 2010)

The polarization of the emission from a set of highly strained *a*-plane GaN/AlN multiple quantum wells of varying well widths has been studied. A single photoluminescence peak is observed that shifts to higher energies as the quantum well thickness decreases due to quantum confinement. The emitted light is linearly polarized. For the thinnest samples the preferential polarization direction is perpendicular to the wurtzite *c* axis with a degree of polarization that decreases with increasing well width. However, for the thickest well the preferred polarization direction is parallel to the *c* axis. Raman scattering, x-ray diffraction, and transmission electron microscopy studies have been performed to determine the three components of the strain tensor in the active region. Moreover, the experimental results have been compared with the strain values computed by means of a model based on the elastic continuum theory. A high anisotropic compressive in-plane strain has been found, namely, −0.6% and −2.8% along the in-plane directions $[1\bar{1}00]$ and [0001], respectively, for the thickest quantum well. The oscillator strength of the lowest optical transition has been calculated within the framework of a multiband envelope function model for various quantum well widths and strain values. The influence of confinement and strain on the degree of polarization is discussed and compared with experiment considering various sets of material parameters.

DOI: 10.1103/PhysRevB.82.125405 PACS number(s): 78.55.Cr, 78.67.De, 73.21.Fg

I. INTRODUCTION

Among the different approaches proposed for the improvement of III-nitride semiconductor optoelectronic devices, the growth of heterostructures along nonpolar directions of the wurtzite structure (*a* and *m* planes) (Ref. 1) has already proven to give very good results in terms of efficiency and stability of the optical emission.[2,3] The many positive consequences of the absence or partial reduction in the internal electric field in nonpolar heterostructures when compared to their polar counterparts include the narrowing of the emission peak, the increase in emission energy, and the lack of blueshift with increasing excitation power. These benefits are especially relevant for improving the optical characteristics of wide quantum wells (QWs),[4,5] quantum dots (QDs),[6] and quantum wires.[7] Another interesting property that stands out in nonpolar structures is their linear optical polarization, arising from the fact that the *c* axis of the wurtzite crystal lies in the growth plane. This anisotropy, inherent in bulk, can be tuned to some extent by the control of strain and confinement[8–13] and has been proposed for the realization of polarization-sensitive photodetectors.[14]

So far, most of the optical studies on nonpolar nitride heterostructures have reported a preferential polarization perpendicular to the *c* axis (hereafter denoted as positive polarization) and a linear degree of polarization (DOP) close to unity, in agreement with theoretical predictions that take into account the complexity of the wurtzite band structure and the anisotropic strain present in the material.[11–14] A partial loss of polarization has been observed in confined systems and attributed to the mixing of valence-band states due to quantum confinement.[6,11–13] Most notably, a preferential polarization of the spontaneous emission parallel to the wurtzite *c* axis has been reported in *a*-plane QD superlattices.[15] This results in a negative degree of polarization that has been ascribed to the combined effect of large values of strain and anisotropic confinement due to the elongated shape of the QDs.

In this work we analyze the emission of a series of highly strained GaN/AlN multiple QWs with various well thicknesses grown along the $[11\bar{2}0]$ direction of the wurtzite structure (*a* plane). The degree of polarization, determined by polarized photoluminescence measurements, is found to decrease with increasing QW thickness, changing sign from positive to negative for a 16-nm-thick QW. To identify the physical conditions that lead to the observed polarization reversal, great care has been taken to determine the anisotropic strain state of the active layers. Combined Raman scattering, transmission electron microscopy (TEM) and x-ray diffraction (XRD) studies reveal out-of-plane expansion as high as 1.5%, comparable to those reported for *a*-plane QDs in Ref. 15. These strain values are significantly larger than in previously studied GaN QWs and films, characterized by strains in the 0.04–0.4 % range.[16] Our results demonstrate that a polarization reversal may take place even in the absence of anisotropic confinement. The role of QW confinement and anisotropic strain in the determination of the character of the valence bands and, consequently, on the polarization of the emission, is analyzed with the aid of theoretical calculations in the framework of an eight-band envelope function model. A discussion of the influence of the values of the material parameters on the theoretical results is also presented.

II. EXPERIMENTAL DETAILS AND THEORETICAL MODELING

Samples were grown by plasma-assisted molecular-beam epitaxy on a commercial *a*-plane 6H-SiC substrate polished

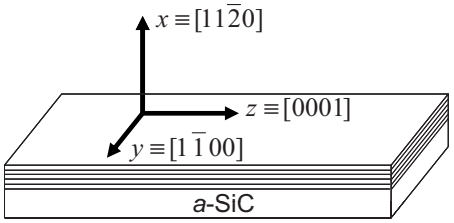

FIG. 1. Schematic showing the orientation of the coordinates x, y, and z with respect to the crystallographic directions of the multiple QW samples.

by NOVASiC. As first step a 50 nm AlN buffer layer was deposited on the substrate. Subsequently, a 5 period multiple QW consisting of GaN wells of thickness d and ~10 nm AlN barriers was grown, with d=2, 4, 8, and 16 nm. Growth was performed at 750 °C, in N-rich conditions, leading to the observation of a streaky reflection high-energy electron diffraction pattern, characteristic of smooth $[11\bar{2}0]$ AlN and GaN surfaces.[17] A schematic of the crystallographic orientation of the samples is shown in Fig. 1. The sample growth direction $[11\bar{2}0]$ is labeled as x while y and z denote the in-plane $[1\bar{1}00]$ and [0001] directions, respectively.

Photoluminescence (PL) measurements were performed using the frequency-doubled line (244 nm) of an Ar^+-ion laser as excitation source. A spectrometer of 0.19 m focal length with 2400 grooves/mm grating and a Si charge-coupled-device detector were used to disperse and detect the PL signal. The spectral resolution was in the range of 3 meV. The samples were mounted in a closed-cycle He cryostat and the temperature was adjusted between 10 K and room temperature. The experiment was performed in backscattering geometry with the wave vector of the emitted light along x. The linear polarization components of the emission along $y(E \perp c)$ and $z(E \| c)$ were measured by keeping a linear polarizer fixed in front of the spectrometer entrance and rotating the samples by means of a special holder. In this way corrections due to the spectral response of the spectrometer were avoided.

Given the decisive influence of strain on the optical properties of the samples, it is of major concern to assess the state of anisotropic strain of the GaN/AlN heterostructures. This has been done with an array of experimental techniques, namely, Raman scattering, TEM, and XRD. For μ-Raman measurements a Jobin-Yvon T64000 triple spectrometer was used. All measurements were performed at room temperature and in backscattering geometry. The 514.53 nm line of an Ar^+-ion laser was the excitation source. A 100× microscope objective (NA=0.90) was used to focus the light on the sample and collect the signal directly to the spectrometer stage through an edge filter. A linear polarizer and a $\lambda/2$ plate were used to perform measurements in crossed and parallel polarization configurations. The excited area on the sample was about 1 μm^2 and the incident power density was kept in the 10^5 W/cm^2 range to avoid sample heating. TEM experiments were carried out on a Jeol 4000EX microscope (Cs=1 mm) operated at 400 kV. Cross-sectioned samples were prepared by mechanical polishing followed by ion milling (PIPS Gatan equipment). X-ray diffraction experiments were performed using a SEIFERT XRD 3003 PTS-HR diffractometer with a beam concentrator prior to a Ge (220) two-bounce monochromator and a 0.2° long plate collimator in front of the detector. The symmetrical $(11\bar{2}0)$ reflection, as well as the off-axis $(11\bar{2}2)$ and $(30\bar{3}0)$ reflections (in incident and grazing incidence) were measured for the determination of the lattice parameters.

In addition to the experimental determination of the strain, it is also interesting to obtain an initial estimate by means of a simple model based on the elastic continuum theory. In this model, the AlN buffer layer and multiple QW structure is assumed to form a coherent free-standing multilayer with the same in-plane lattice parameters throughout the whole structure. Consequently, we have not taken into account the possibility of a significant plastic relaxation. It should be noted that this hypothesis is fully supported by TEM observations reported later in the present work. By imposing the condition of minimum elastic energy under the above assumptions, the coherent in-plane lattice parameters and strain components of the planar GaN/AlN heterostructure can be obtained easily. In the calculations we have referred all the results to the system of axes described in Fig. 1. The theoretical results for the in-plane strains, $\varepsilon_{yy}^{(k)}$ and $\varepsilon_{zz}^{(k)}$, and out-of-plane strain $\varepsilon_{xx}^{(k)}$ (where the index k labels the material, AlN or GaN) can be found in the Appendix. The total material thicknesses d_{GaN} and d_{AlN} appearing in the expression of the strains are the same as in the structure studied experimentally, namely, $d_{GaN}=5\times d$ and $d_{AlN}=50$ nm+5 $\times 10$ nm.

The electronic structure of the MQW samples has been analyzed by means of an eight-band envelope function model, that includes the strain influence through the electronic deformation-potential (Bir-Pikus) theory.[18,19] The quantum confinement is introduced through the offset between GaN and AlN valence-band edges [VBO=0.5 eV (Ref. 20)]. For computational convenience the multiple QW is treated as an infinitely periodic superlattice so that the envelope function can be expanded in plane waves. Due to the high barriers in the GaN/AlN system, no electronic inter-well coupling is observed in the calculations, and we are thus confident that the results so obtained for the lowest (highest) conduction (valence) band states are representative of the finite multiple QW investigated experimentally. Given the negligible barrier penetration, we have taken the GaN parameters for the whole structure. Nevertheless, a critical point hampering this kind of calculations is the lack of consensus on a reliable set of Luttinger-type parameters A_i and deformation potentials D_i.[21] The situation is worsened by the fact that some results, as will be shown below, seem to be very sensitive to those parameters. To illustrate this, the calculations have been performed considering two sets of parameters. The first set (Set 1) is taken from Ref. 19. The origin of the values is diverse, but in general they have been obtained by fitting various optical spectra, always resorting to the quasicubic approximation. The A_i subset is very similar to the set of values recommended in Ref. 21 and is widely used in theoretical calculations. On the other hand, the second set of parameters (Set 2) is taken from a recent fit of bulk band-structure state-of-the-art *ab initio* calculations by means of

the eight-band $\mathbf{k}\cdot\mathbf{p}$ model.[22,23] To disentangle the interband hydrostatic deformation potentials reported in Ref. 23 ($a_{cz}-D_1=-5.81$ eV and $a_{ct}-D_2=-8.92$ eV) into its conduction- and valence-band contributions, we have fixed the conduction-band deformation potentials to the value reported in Ref. 24 for cubic GaN, so that $a_{cz}=a_{ct}=-4.59$ eV. The main features of Set 2 are its internal consistency and the fact that no use of the cubic approximation has been made.

From the calculated conduction- and valence-subband structures, we are particularly interested in the interband transition energies and wave functions at $(k_y,k_z)=(0,0)$. These wave functions are generally written as eight-component spinors, $\Psi=\Sigma_j F_j(x)|u_j\rangle$, where $F_j(x)$ are the envelope functions and $|u_j\rangle$ run over the eight Bloch functions used as a basis in the theoretical model, $|S,\sigma\rangle$, $|X,\sigma\rangle$, $|Y,\sigma\rangle$, $|Z,\sigma\rangle$, $\sigma=\uparrow,\downarrow$. The polarization-dependent oscillator strengths are then given by (Ref. 10),

$$f_\alpha=\left|\sum_{j,m}\left[\int dx F_j^{(c)}(x)F_m^{(v)}(x)\right]\langle u_j|p_\alpha|u_m\rangle\right|^2. \quad (1)$$

Here, the labels (c) and (v) refer to the lowest conduction-band and highest valence-band confined states, respectively. The polarization features of the measured luminescence are compared below with the theoretical degree of polarization,

$$(\mathrm{DOP})_{\mathrm{th}}=\frac{f_y-f_z}{f_y+f_z}. \quad (2)$$

Finally, we would like to notice that excitonic effects, not taken into account in our calculations, will surely change the optical transition energies, but they are not expected to appreciably modify the oscillator strengths.

III. RESULTS AND DISCUSSION

Low-temperature PL spectra of the four samples studied are shown in Fig. 2(a). For each sample the spectra corresponding to polarization components perpendicular and parallel to the c axis are plotted. The intensity of each set of spectra has been rescaled at convenience to improve the legibility of the figure. As the QW thickness increases, the expected redshift of the emission peak is observed as a result of decreasing quantum confinement, with no trace of the Stark effect characteristic of QWs grown along the c axis. This shift is shown in the inset together with the theoretical calculations of the lowest-energy optical transition. It is reasonable that the experimental data lie below the theoretical calculations since the exciton binding energy is not taken into account. Furthermore, a Stokes shift is expected due to QW thickness fluctuation. Recently, Badcock *et al.*[13] reported that the combined effect of excitonic binding energies and Stokes shift lead to a shift in the range of 50–100 meV for a-plane $GaN/Al_{0.18}Ga_{0.82}N$ QWs. Although precise estimation of these effects is difficult to make in our case, we expect them to lie in the same range. Indeed, the inset in Fig. 2(a) illustrates that experimental results can be reasonably fitted by shifting the calculations by 100 meV. Additionally, we observe that the width of the emission decreases from 240 meV for the 2 nm QW to 100 meV for the 16 nm sample. This

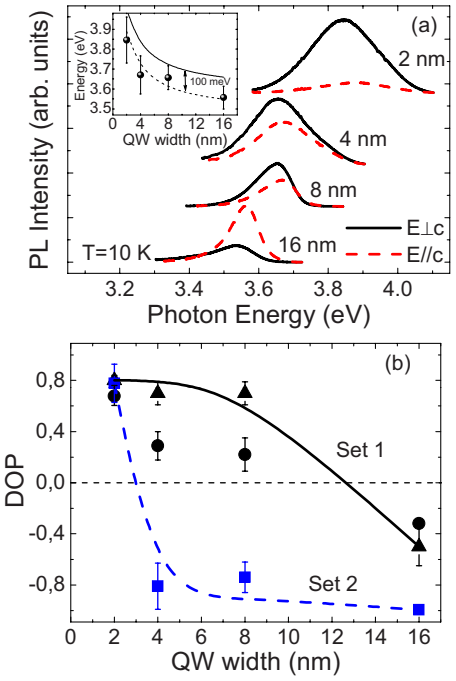

FIG. 2. (Color online) (a) Low-temperature PL spectra of the four multiple QWs with width (d) varying from 2 to 16 nm. Full lines correspond to $E\perp c$ and dashed lines to $E\|c$. The inset shows the peak energy as a function of QW width (dots) together with the theoretical results obtained by using the parameters of Set 1 (full line). The dashed line results from redshifting the theoretical calculations by 100 meV. (b) DOP vs QW width. Dots correspond to the experimental values. Triangles show the result of calculations using the parameters of Set 1 while squares correspond to Set 2. Lines are guide to the eyes.

trend is also characteristic of inhomogeneous broadening due to fluctuations in QW width and strain. In any case, as expected from the lack of internal electric field, the width is considerably smaller than that reported for 2-nm-wide c-plane GaN/AlN QWs,[25] which is around 350 meV.

The most relevant feature of the spectra is related to the evolution of the polarized components of the PL with QW width. The emission of the 2 nm QW is dominated by $E\perp c$ component. As the QW width increases, the relative intensity of the $E\|c$ polarization increases, and for the 16 nm QW this component eventually dominates the emission. Besides, in the $E\|c$ polarization the emission is shifted between 15 and 25 meV to higher energies in comparison to the $E\perp c$ polarized PL spectrum. To quantify the degree of polarization we introduce the quantity $\mathrm{DOP}=(I_y-I_z)/(I_y+I_z)$, where I_y and I_z are the integrated intensities for the emission polarized perpendicular and parallel to the c axis, respectively. The values of DOP corresponding to the PL spectra of Fig. 2(a) are shown in Fig. 2(b) (dots). The DOP decreases as the QW width is increased, starting from large positive values (0.7 for the 2 nm QW) and showing a clear sign reversal (−0.3) for the 16 nm well. Identical results were obtained after exciting the PL on another spot on the sample and by measuring the emitted light by means of a different setup (0.46 m spectrometer focal length, 600 grooves/mm gratings, and a $\lambda/2$ plate). Small differences in the DOP obtained in both

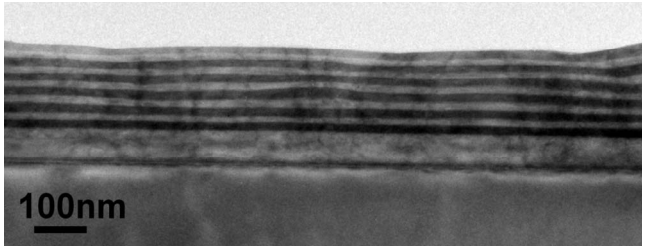

FIG. 3. Low-resolution TEM image of the 16 nm QW sample along [0001] zone axis showing the morphology of the multiple QWs.

measurements are taken into account in the error bars of Fig. 2(b). Additionally, temperature-dependent PL measurements indicate that the DOP weakly depends on the temperature. This is an indication that it is not significantly affected by localization that is likely to occur in QW structures at low temperature. At first glance the observed trend is quite unexpected. An increase in the quantum well width from 2 to 16 nm reduces considerably the quantum confinement effects. Consequently, polarization values close to those found in bulk ($\sim$1), could be intuitively foreseen. As we will see later in the discussion, the dominant influence of strain over confinement on the character of the valence bands plays against this simple picture.

The two samples containing the 2 and 16 nm QWs have been studied by TEM along both $[1\bar{1}00]$ and [0001] zone axes. Low magnification images (see Fig. 3) have revealed the anisotropic morphology of the QWs, which appear wavy,[17] with undulations starting from the first AlN/GaN interface. Due to the absence of correlation in the rugosity of successive AlN layers, the width of the QWs varies, up to 20%. For the two samples, high-resolution TEM (HRTEM) images were taken along both zone axes (see in Fig. 4 images taken along [0001] zone axis) and analyzed with the

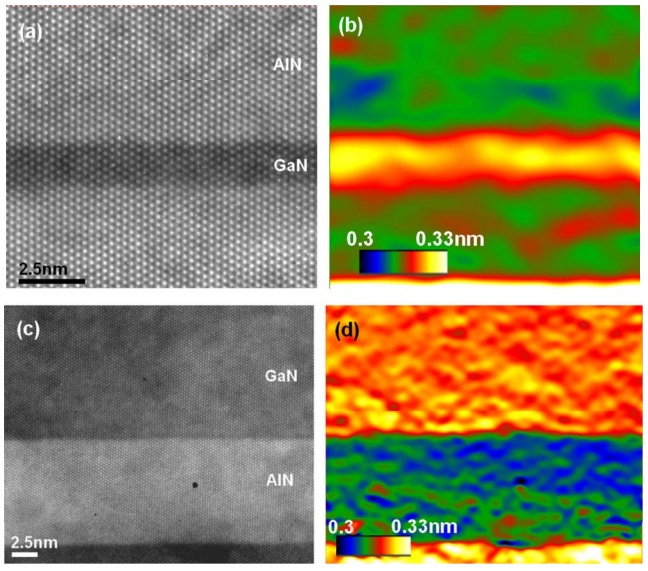

FIG. 4. (Color online) HRTEM images taken along the [0001] zone axis and corresponding map of a_x obtained from GPA analysis: [(a) and (b)] 2 nm QW and [(c) and (d)] 16 nm QW.

geometrical phase analysis (GPA) method[26] in order to get the lattice parameters c, a_x, and a_y and therefore the strain maps at the atomic scale. Analysis of the (0002) reflection did not show any difference between c parameters of SiC, AlN (either in the buffer or the multiple QW), and GaN. Therefore we conclude that $c_{GaN}=c_{AlN}=0.504$ nm, which is the value reported for $c/3$ of bulk SiC. Values of a_x and a_y were obtained from images taken along the [0001] zone axis that allowed the evaluation of the various strain tensor components. No significant difference was detected for a_y between AlN and GaN either, and the values were checked to satisfy the Poisson relation. The corresponding values of the strain components for GaN were found to be $\varepsilon_{xx}=1.6\%$, $\varepsilon_{yy}=-2.5\%$, and $\varepsilon_{zz}=-2.8\%$ for the 2 nm QW, and $\varepsilon_{xx}=1.0\%$, $\varepsilon_{yy}=-0.6\%$, and $\varepsilon_{zz}=-2.8\%$ for the 16 nm QW. These values were obtained with accuracy of 0.1%. GPA analysis indicates that the influence of QW thickness fluctuations on these strain values is negligible. The data show a marked relaxation of ε_{yy} as the width of the QW increases while the value of ε_{zz} remains constant.

It should be mentioned at this stage that anisotropic morphology is commonly observed in nonpolar AlN (Refs. 27 and 28) and AlN/GaN heterostructures[17] grown on a-plane SiC substrates. Such an anisotropic morphology is assigned to the anisotropic strain state of AlN ($\Delta a/a=-1.00\%, \Delta c/c=+1.17\%$) and GaN ($\Delta a/a=-3.39\%, \Delta c/c=-2.81\%$) with respect to a-plane SiC, which accordingly leads to an anisotropic strain relaxation mechanism. As a matter of fact, it has been found that a-plane AlN layers grown on a-plane SiC were almost fully strained along both [0001] and $[1\bar{1}00]$ directions for thicknesses up to at least 100 nm.[29] In the present case, conventional XRD analysis of the samples allowed one to determine the in-plane lattice parameters a_y and c of the AlN buffer layers. Results show that for all the samples the AlN buffer layer is strained by the SiC substrate. Along the y direction it is partially compressed by the SiC giving place to a $\Delta a/a$ between -0.5% and -0.8%. Along the c axis it is totally expanded to the SiC value, yielding to a $\Delta c/c$ of $+1.17\%$, consistent with the further experimental evidence that the c parameter for both multiple QWs studied by TEM was equal to that of SiC.

Raman-scattering experiments were performed to determine the orientation of the c axis on the sample surface prior to PL measurements and to analyze the evolution of strain in the samples. The selection rules are very well fulfilled in all samples and allow the clear assignment of the various modes for GaN and AlN. All modes attributed to GaN are strongly blueshifted (circa 30 cm^{-1}) with respect to their relaxed bulk values,[30] as a consequence of the compressive in-plane strain in the GaN layers. The AlN barriers, on the other hand, experience a smaller tensile strain evidenced by a redshift of around 5 cm^{-1} of the phonon modes. Separate modes corresponding to the AlN barriers and buffer could only be resolved for $d=16$ nm. The evolution of the frequency of the phonon modes is shown in Fig. 5 as a function of quantum well width. As d increases there is a small but clear shift of the modes to lower frequencies, that is, toward their relaxed values, evidencing a progressive relaxation of strain in thicker QWs.

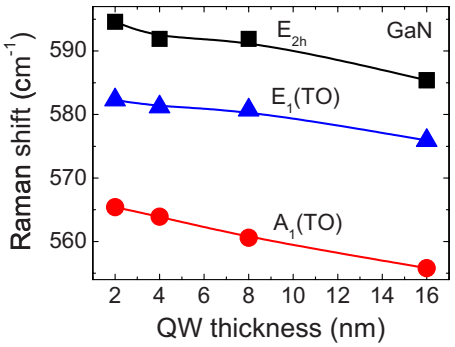

FIG. 5. (Color online) Raman shift of E_{2h} (squares), E_1(TO) (triangles), and A_1(TO) (dots) phonon modes of GaN as a function of QW width. The lines are guide to the eyes.

We have quantified the values of the strain tensor from the frequency of the E_{2h} and A_1(TO) phonon modes. The choice of this pair of modes is justified by the analysis of the relative values of the GaN deformation potentials.[31] The phonon mode frequencies have been related to strain through the deformation-potential approximation, $\Delta\omega = a(\varepsilon_{xx}+\varepsilon_{yy})+b\varepsilon_{zz}$, where $\Delta\omega$ is the frequency shift with respect to the unstrained value[30] and a and b the phonon deformation potentials.[31] Finally, assuming that the structure grows stress free along $[11\bar{2}0]$ and using the Poisson relation, it is possible to obtain values of the three diagonal strain tensor components. It should be emphasized that this procedure is fully justified by TEM results where in-plane and out-of-plane lattice parameters are found to be consistently related through the Poisson's relationship. The strain values derived from the analysis of the Raman spectra are plotted in Fig. 6 (empty symbols) together with XRD/TEM combined results (full symbols) and the theoretical calculations (lines). The calculated strain values show that the GaN layers are strongly compressed along z and y (in-plane directions) and tensile strained along x, in agreement with XRD/TEM and Raman results. As the well thickness is increased from 2 to 16 nm, calculations show that the strain values are expected to decrease by a factor 2. The comparison with XRD/TEM results indicates that while the relaxation of ε_{yy} and ε_{xx} approximately follows the elastic trend, ε_{zz} remains constant at the value imposed by the SiC substrate. In agreement with XRD/TEM, Raman data indicate a larger relaxation of the ε_{yy} component as the QW width increases, while changes in ε_{zz} are much smaller. However, strain values obtained by Raman underestimate the in-plane compression, especially along z. As commented earlier, the anisotropic relaxation observed experimentally may be understood to some extent by considering the high energy necessary for the activation of pyramidal slip systems along [0001], in $[11\bar{2}0]$ oriented AlN.[29] Based on a similar model as the one described in the Appendix, it is possible to calculate the elastic influence of the SiC substrate on the superlattice strain state. Inclusion of a SiC layer effectively decreases the value of ε_{zz} of the GaN well toward the GaN-SiC lattice mismatch (−2.8%). However, the effect of this layer on ε_{yy} is even larger since the lattice mismatch along y is as large as −3.4%.

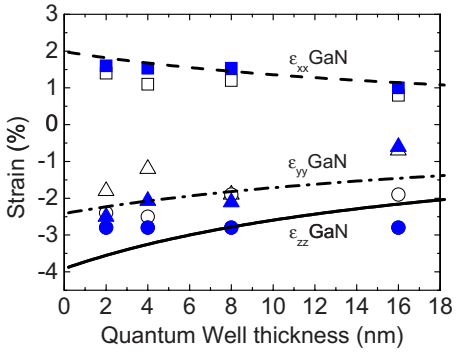

FIG. 6. (Color online) Comparison between experimental (full symbols for XRD/TEM, empty for Raman) and theoretical (lines) values of strain as a function of QW width. Squares show the expansion along the growth direction x while triangles and dots correspond to the in-plane compression along y and z, respectively.

We turn now our attention to the effect of strain and confinement on the polarization of the optical transitions. It is well known that the upper most valence bands of wurtzite GaN are mainly constructed from atomic p_x, p_y, and p_z orbitals. At the Γ point the topmost valence band (heavy-hole band), presents $p_x \pm ip_y$ atomic character so that it can be described by $|X \pm iY\rangle$ Bloch wave functions.[18] Taking into consideration the spin-orbit coupling, the second (light hole, LH) and third (split-off crystal-field hole, CH) bands couple together. As a result, besides p_x and p_y character, the LH band presents a small p_z contribution (its Bloch function has a small $|Z\rangle$ component). Conversely, the CH band presents a predominant p_z character with a small contribution from p_x, and p_y orbitals. Optical transitions involving these three valence bands are usually denoted as A, B, and C excitons, in order of increasing energy. Due to the character of the corresponding valence bands, the emission originated by the recombination of these excitons will be strongly polarized along the c axis only for exciton C. Therefore, the polarization dependence of the oscillator strength can be strongly altered not only by strain but also by confinement. For analyzing the relative importance of these effects we have used the model presented in Sec. II to compute the polarization components of the oscillator strength of the lowest-energy interband transition, f_α [see Eq. (1)], as a function of strain for both bulk GaN and the 2 nm GaN/AlN quantum well sample. Only the in-plane strain components, ε_{yy} and ε_{zz}, are varied, and following the discussion above, the strain component along the growth direction, ε_{xx}, is obtained through Poisson's equation. For these calculations, the material parameters of Set 1 have been used. The results are displayed in Fig. 7 for bulk GaN and the 2 nm QW. The oscillator strength represented corresponds to the lowest-energy transitions polarized along y (f_y) [(a) and (c)] and along z (f_z) [(b) and (d)]. Surprisingly, bulk and QW oscillator strengths are almost identical provided that $\varepsilon_{yy} < -0.5\%$, as it is the case in our samples, indicating negligible influence of the confinement for this set of parameters. We have checked that, as expected, this similarity increases for thicker QWs. As pointed out by Yamaguchi[32] in the special case of isotropic in-plane strain, this can be attributed to the similar values taken by the valence-band Luttinger-type parameters A_4 and

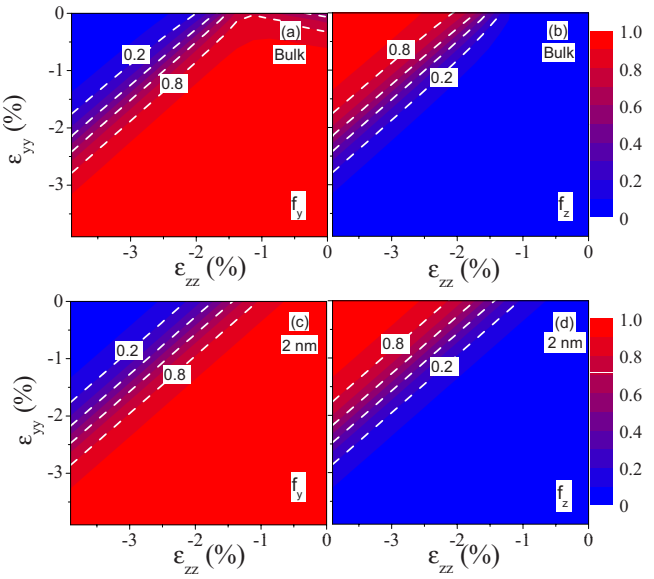

FIG. 7. (Color online) [(a) and (c)] Oscillator strengths f_y and [(b) and (d)] f_z mapped as a function of in-plane strain. The figures correspond to bulk GaN (top) and to the 2 nm QW (bottom). Parameters of Set 1 were used. Contour lines are plotted at intervals of 0.2.

A_5. The analysis of the figure indicates that the emission would be polarized along the c axis provided that the compression along z is large while the one along y is sufficiently small. As shown in Fig. 6, Raman, TEM, and XRD measurements reveal that these conditions are fulfilled only for the 16 nm QW. Consequently, the theoretical calculation would predict a negative degree of polarization $(\mathrm{DOP})_{\mathrm{th}}<0$ [see Eq. (2)] for the emission of this sample. On the contrary, the emission of thinner QWs, subject to larger compression along y, is predicted to be polarized perpendicular to the c axis [positive $(\mathrm{DOP})_{\mathrm{th}}$]. The conditions required for a negative DOP and the influence of strain can be better appreciated in Fig. 8(a), where we have plotted the $(\mathrm{DOP})_{\mathrm{th}}$ of a 16 nm QW as a function of in-plane strain, together with the values of strain determined by TEM for the 2-nm- and 16-nm-thick QWs. The contour lines $(\mathrm{DOP})_{\mathrm{th}}=0$, corresponding to unpolarized emission, is marked in white and separates negative

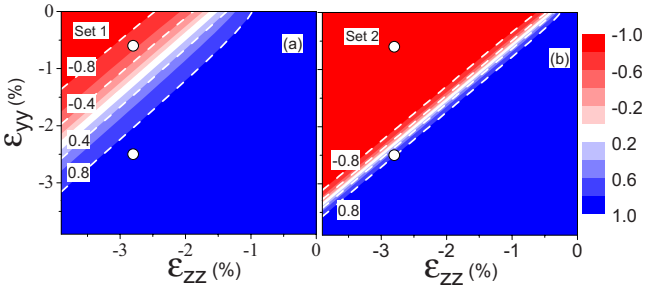

FIG. 8. (Color online) Calculated $(\mathrm{DOP})_{\mathrm{th}}$ mapped as a function of in-plane strain for a 16 nm GaN/AlN a-plane QW obtained by using the parameters of (a) Set 1 and (b) Set 2. The full line marks $(\mathrm{DOP})_{\mathrm{th}}=0$. The open circles correspond to the values of strain obtained by TEM for the 2 nm (lower point) and the 16 nm QWs (upper point).

(upper left corner, red online) from positive $(\mathrm{DOP})_{\mathrm{th}}$ (blue online). We can appreciate that the polarization sign reversal takes place smoothly, since the change from 0.8 to −0.8 covers a large range of strain. This ensures a gradual change in polarization as the strain in the QWs is relaxed, in very good accordance with PL experiments that indicate a slow change in the DOP as a function of QW thickness.

Nevertheless, the validity of this analysis may change depending on the values of the material parameters used in the model. With the aim of giving a glimpse of these changes, a similar $(\mathrm{DOP})_{\mathrm{th}}$ contour map was obtained by using the parameters of Set 2 [Fig. 8(b)]. There are two main differences when compared with the results of Set 1. First, the line that marks the polarization reversal shifts considerably toward larger (in absolute value) ε_{yy} (smaller ε_{zz}) for Set 2. As a consequence, the strain characteristics of QWs with thicknesses of 4, 8, and 16 nm would lead to a negative $(\mathrm{DOP})_{\mathrm{th}}$, in clear disagreement with the experimental evidence. Second, the polarization sign reversal takes place very abruptly when the parameters of Set 2 are used, a prediction inconsistent with our PL measurements. This difference between the calculated $(\mathrm{DOP})_{\mathrm{th}}$ of Sets 1 and 2 is attributed to the smaller absolute value of the deformation potentials used in Set 1. For a better comparison of our PL results with the theory we have plotted in Fig. 2(b) the $(\mathrm{DOP})_{\mathrm{th}}$ calculated with parameters from Sets 1 and 2. In these calculations the QW width has been kept constant to 16 nm and strain corresponds to that determined by TEM. The error bars on the calculated points reflect changes due to the uncertainties in the determination of strain. Similarly as in the experiment, the DOP calculated with the parameters of Set 1 changes gradually from positive to negative values. The calculations performed with Set 2 predict a very abrupt change in the DOP, in disagreement with our PL results. As a matter of fact the general conclusions obtained with other sets of parameters[10,21] are very similar to those of Set 2: they display an abrupt sign reversal and, as in Set 1, negligible confinement effects. Only the parameters of Ref. 33 reflect a strong dependence of the polarization on QW width, which is attributed to the large difference between the valence-band parameters A_4 and A_5. Analysis of the higher-energy optical transitions also reveals important differences between results of Set 1 and Set 2, that are specially relevant in the region of strain characteristic of the 16-nm-thick QW ($\varepsilon_{zz}=-2.8\%$ and $\varepsilon_{yy}=-0.6\%$). For Set 1 the fundamental and first excited transitions, separated by 12 meV, have opposite dominant character (p_z and p_y, respectively). On the contrary, for Set 2 both transitions have the same character, p_y, and it is not until the fourth excited transition, 100 meV apart, that we find the experimentally observed p_z character. From our calculations it is clear that the character of the transitions is very sensitive to the values of the deformation potentials chosen. With this respect, it is important to remind that, as indicated in Sec. II, the values of D_1 and D_2 used in this work for Set 2 are extracted from those reported in Refs. 22 and 23 by fixing the conduction-band deformation potentials to −4.59 eV, adequate for GaN with cubic symmetry. Our result should encourage the scientific community to provide reliable independent values of the conduction- and valence-band deformation potentials.

Finally, we would like to point out that the influence of the out-of-plane strain component, ε_{xx}, on the polarization characteristics is much smaller than that of ε_{yy} and ε_{zz}. Changes of 10% in the value of ε_{xx} resulted in variations of only 0.1% in the DOP. A complete study of the strain state of a sample with special care in the determination of the in-plane strain tensor components is therefore essential to relate electronic states and strain characteristics.

IV. CONCLUSIONS

In this paper we have studied the polarized emission and strain state of *a*-plane GaN/AlN multiple QWs with well thickness ranging from 2 to 16 nm. It is shown that the degree of polarization gradually decreases from 0.7 for the thinnest QW to −0.3 for the 16 nm well. A combined analysis performed by XRD, Raman, and TEM shows that the value of the ε_{zz} strain component is determined by the SiC substrate and does not change appreciably in the different samples, taking a value of −2.8%. The relaxation along the *y* axis is larger. The ε_{yy} compression decreases from −2.5% for the 2 nm sample to −0.6% for the thickest QW while expansion along the growth direction *x* was found to fulfill the Poisson relation. The oscillator strength of the different polarization components was analyzed by means of an eight-band $\mathbf{k}\cdot\mathbf{p}$ model and using two different sets of parameters. Our results indicate that the character of the lowest-energy transition is independent of the QW width. Indeed, it is the value of ε_{zz} and ε_{yy} strain tensor components which determine the degree of polarization while variations in ε_{xx} have a minor effect. Negative values of polarization are obtained when compression along *z* is large while that along *y* is considerably smaller. These requirements are confirmed by comparison of the calculations with the experimental strain and polarization of our samples. Calculations made using the parameters of Set 1 (Ref. 19) reproduce the evolution of the polarization measured for the different samples to a better extent than other sets that result in a negative polarization for three of the samples, in contradiction with the observations.

ACKNOWLEDGMENTS

This work was supported by Project No. MAT2009-010350 (Ministry of Science and Innovation of Spain, FEDER) and the Generalitat Valenciana.

APPENDIX: ELASTIC MODEL OF STRAIN

Our theoretical model for the strain considers a multilayer system composed of alternated layers of two materials with hexagonal symmetry, labeled as $k=1,2$, with bulk lattice parameters (a_k, c_k) and elastic constants $C_{ij}^{(k)}$. The *c* axis of both materials is parallel and lies on the layer planes. The lattice mismatches between both materials are defined as follows:

$$\varepsilon_a = \frac{a_1}{a_2} - 1 \quad \text{and} \quad \varepsilon_c = \frac{c_1}{c_2} - 1.$$

For the calculations presented in this paper, the numerical values of the various material parameters are taken from Ref. 21. We have taken $k=1$ for AlN and $k=2$ for GaN. Therefore, $\varepsilon_a = -0.0241$ and $\varepsilon_c = -0.0391$.

The multilayer in-plane lattice parameters, a_y and c can be obtained by solving the system of equations derived from the elastic equilibrium condition:

$$\begin{pmatrix} \frac{C_x^{(1)}}{a_1^2}d_1 + \frac{C_x^{(2)}}{a_2^2}d_2 & \frac{C_y^{(1)}}{a_1 c_1}d_1 + \frac{C_y^{(2)}}{a_2 c_2}d_2 \\ \frac{C_y^{(1)}}{a_1 c_1}d_1 + \frac{C_y^{(2)}}{a_2 c_2}d_2 & \frac{C_z^{(1)}}{c_1^2}d_1 + \frac{C_z^{(2)}}{c_2^2}d_2 \end{pmatrix} \begin{pmatrix} a_y \\ c \end{pmatrix} = \begin{pmatrix} \frac{(C_x^{(1)} + C_y^{(1)})}{a_1}d_1 + \frac{(C_x^{(2)} + C_y^{(2)})}{a_2}d_2 \\ \frac{(C_y^{(1)} + C_z^{(1)})}{c_1}d_1 + \frac{(C_y^{(2)} + C_z^{(2)})}{c_2}d_2 \end{pmatrix},$$

where d_k is the total width of material *k*,[34] and

$$C_x^{(k)} = C_{11}^{(k)} - \frac{(c_{12}^{(k)})^2}{c_{11}^{(k)}},$$

$$C_y^{(k)} = C_{13}^{(k)} - \frac{c_{12}^{(k)} c_{13}^{(k)}}{c_{11}^{(k)}},$$

$$C_z^{(k)} \to C_{33}^{(k)} - \frac{(c_{13}^{(k)})^2}{c_{11}^{(k)}}.$$

The above system can be easily solved numerically but for completeness we also present the analytic solution that can be obtained after some algebraic manipulations,

$$a_y = K_1^{(a)} a_1 + K_2^{(a)} a_2,$$

$$c = K_1^{(c)} c_1 + K_2^{(c)} c_2,$$

where

$$K_1^{(a)} = \frac{\frac{1}{(1+\varepsilon_a)(1+\varepsilon_c)}[C_x^{(1)} C_z^{(1)} - (C_y^{(1)})^2]d_1^2 + \left[\frac{1}{(1+\varepsilon_c)} C_z^{(1)}(C_x^{(2)} + C_y^{(2)}) - (C_y^{(1)} + C_z^{(1)}) C_y^{(2)}\right] d_1 d_2}{\mathbb{D}},$$

$$K_2^{(a)} = \frac{(1+\varepsilon_a)(1+\varepsilon_c)[C_x^{(2)} C_z^{(2)} - (C_y^{(2)})^2]d_2^2 + [(1+\varepsilon_c)(C_x^{(1)} + C_y^{(1)}) C_z^{(2)} - C_y^{(1)}(C_y^{(2)} + C_z^{(2)})] d_1 d_2}{\mathbb{D}},$$

$$K_1^{(c)} = \frac{\frac{1}{(1+\varepsilon_a)(1+\varepsilon_c)}[C_x^{(1)}C_z^{(1)} - (C_y^{(1)})^2]d_1^2 + \left[\frac{1}{(1+\varepsilon_a)}C_x^{(1)}(C_y^{(2)} + C_z^{(2)}) - (C_x^{(1)} + C_y^{(1)})C_y^{(2)}\right]d_1d_2}{\mathbb{D}},$$

$$K_2^{(c)} = \frac{(1+\varepsilon_a)(1+\varepsilon_c)[C_x^{(2)}C_z^{(2)} - (C_y^{(2)})^2]d_2^2 + [(1+\varepsilon_a)(C_y^{(1)} + C_z^{(1)})C_x^{(2)} - C_y^{(1)}(C_x^{(2)} + C_y^{(2)})]d_1d_2}{\mathbb{D}},$$

and

$$\mathbb{D} = \frac{1}{(1+\varepsilon_a)(1+\varepsilon_c)}[C_x^{(1)}C_z^{(1)} - (C_y^{(1)})^2]d_1^2 + (1+\varepsilon_a)(1+\varepsilon_c) \times [C_x^{(2)}C_z^{(2)} - (C_y^{(2)})^2]d_2^2 + \left[\frac{(1+\varepsilon_c)}{(1+\varepsilon_a)}C_x^{(1)}C_z^{(2)} + \frac{(1+\varepsilon_a)}{(1+\varepsilon_c)}C_z^{(1)}C_x^{(2)} - 2C_y^{(1)}C_y^{(2)}\right]d_1d_2.$$

Note that, as expected, the equilibrium lattice parameters can be written as a weighted combination of the constituent bulk lattice constants. Nevertheless, the corresponding weights are given by nontrivial expressions involving the thicknesses d_k the elastic constants $C_{ij}^{(k)}$, and the mismatches ε_a and ε_c. This is in contrast with some crude approximations that substitute those weighting factors by the relative volumes of both constituents, i.e., $K_k^{(a)} = K_k^{(c)} = \frac{d_k}{d_1+d_2}$.

Once a_y and c are obtained, the in-plane strains can be calculated from

$$\varepsilon_{yy}^{(k)} = \frac{a_y - a_k}{a_k} \quad \text{and} \quad \varepsilon_{zz}^{(k)} = \frac{c - c_k}{c_k}.$$

Since the structure is assumed to be stress free along the $x \| [11\bar{2}0]$ direction, it is possible to obtain the out-of-plane strain component by using the Poisson relation in each material,

$$\varepsilon_{xx}^{(k)} = \frac{a_x^{(k)} - a_k}{a_k} = -\frac{c_{12}^{(k)}}{c_{11}^{(k)}}\varepsilon_{yy}^{(k)} - \frac{c_{13}^{(k)}}{c_{11}^{(k)}}\varepsilon_{zz}^{(k)}.$$

Here $a_x^{(k)}$ denotes the out-of-plane equilibrium lattice parameter in material k.

[1] P. Waltereit, O. Brandt, A. Trampert, H. T. Grahn, J. Menninger, M. Ramsteiner, M. Reiche, and K. H. Ploog, Nature (London) **406**, 865 (2000).
[2] M. C. Schmidt, K.-C. Kim, H. Sato, N. Fellows, H. Masui, S. Nakamura, S. P. DenBaars, and J. S. Speck, Jpn. J. Appl. Phys., Part 2 **46**, L126 (2007).
[3] M. C. Schmidt, K.-C. Kim, R. M. Farrell, D. F. Feezell, D. A. Cohen, M. Saito, K. Fujito, J. S. Speck, S. P. DenBaars, and S. Nakamura, Jpn. J. Appl. Phys., Part 2 **46**, L190 (2007).
[4] M. D. Craven, P. Waltereit, J. S. Speck, and S. P. DenBaars, Appl. Phys. Lett. **84**, 496 (2004).
[5] M. V. Kisin, R. G. W. Brown, and H. S. El-Ghoroury, Appl. Phys. Lett. **94**, 021108 (2009).
[6] N. Garro, A. Cros, J. A. Budagosky, A. Cantarero, A. Vinattieri, M. Gurioli, S. Founta, H. Mariette, and B. Daudin, Appl. Phys. Lett. **87**, 011101 (2005).
[7] J. Renard, B. Amstatt, C. Bougerol, E. Bellet-Amalric, B. Daudin, and B. Gayral, J. Appl. Phys. **104**, 103528 (2008).
[8] B. Gil and A. Alemu, Phys. Rev. B **56**, 12446 (1997).
[9] A. Alemu, B. Gil, M. Julier, and S. Nakamura, Phys. Rev. B **57**, 3761 (1998).
[10] S. Ghosh, P. Waltereit, O. Brandt, H. T. Grahn, and K. H. Ploog, Phys. Rev. B **65**, 075202 (2002).
[11] B. Rau, P. Waltereit, O. Brandt, M. Ramsteiner, and K. H. Ploog, Appl. Phys. Lett. **77**, 3343 (2000).
[12] Y. J. Sun, O. Brandt, M. Ramsteiner, H. T. Grahn, and K. H. Ploog, Appl. Phys. Lett. **82**, 3850 (2003).
[13] T. J. Badcock, P. Dawson, M. J. Kappers, C. McAleese, J. L. Hollander, C. F. Johnston, D. V. Sridhara Rao, A. M. Sanchez, and C. J. Humphreys, J. Appl. Phys. **105**, 123112 (2009).
[14] S. Ghosh, O. Brandt, H. T. Grahn, and K. H. Ploog, Appl. Phys. Lett. **81**, 3380 (2002).
[15] R. Mata, N. Garro, A. Cros, J. A. Budagosky, A. García-Cristóbal, A. Vinattieri, M. Gurioli, S. Founta, E. Bellet-Amalric, and B. Daudin, Phys. Status Solidi C **6**, S541 (2009).
[16] P. Misra, U. Behn, O. Brandt, H. T. Grahn, B. Imer, S. Nakamura, S. P. DenBaars, and J. S. Speck, Appl. Phys. Lett. **88**, 161920 (2006).
[17] S. Founta, C. Bougerol, H. Mariette, B. Daudin, and P. Vennegues, J. Appl. Phys. **102**, 074304 (2007).
[18] S. L. Chuang and C. Chang, Phys. Rev. B **54**, 2491 (1996).
[19] A. D. Andreev and E. P. O'Reilly, Phys. Rev. B **62**, 15851 (2000).
[20] S. W. King, C. Ronning, R. F. Davis, M. C. Benjamin, and R. J. Nemanich, J. Appl. Phys. **84**, 2086 (1998).
[21] I. Vurgaftman and J. R. Meyer, J. Appl. Phys. **94**, 3675 (2003).
[22] Q. Yan, P. Rinke, M. Scheffler, and C. G. Van de Walle, Appl. Phys. Lett. **95**, 121111 (2009).
[23] Patrick Rinke, M. Winkelnkemper, A. Qteish, D. Bimberg, J. Neugebauer, and M. Scheffler, Phys. Rev. B **77**, 075202 (2008).
[24] Y.-H. Li, X. G. Gong, and S.-H. Wei, Phys. Rev. B **73**, 245206 (2006).
[25] C. Adelmann, E. Sarigiannidou, D. Jalabert, J.-L. Rouvière, B. Daudin, S. Fanget, C. Bru-Chevallier, T. Shibata, and M. Tanaka, Appl. Phys. Lett. **82**, 4154 (2003).
[26] M. J. Hÿtch, E. Snoeck, and R. Kilaas, Ultramicroscopy **74**, 131

(1998).
[27] N. Onojima, J. Suda, and H. Matsunami, Jpn. J. Appl. Phys., Part 2 **41**, L1348 (2002).
[28] M. D. Craven, F. Wu, A. Chakraborty, B. Imer, U. K. Mishra, S. P. Den-Baars, and J. S. Speck, Appl. Phys. Lett. **84**, 1281 (2004).
[29] P. Vennéguès, S. Founta, H. Mariette, and B. Daudin, Jpn. J. Appl. Phys. **49**, 040201 (2010).
[30] H. Harima, J. Phys.: Condens. Matter **14**, R967 (2002).
[31] V. Yu. Davydov, N. S. Averkiev, I. N. Goncharuk, D. K. Nelson, I. P. Nikitina, A. S. Polkovnikov, A. N. Smirnov, M. A. Jacobson, and O. K. Semchinova, J. Appl. Phys. **82**, 5097 (1997).
[32] A. A. Yamaguchi, Jpn. J. Appl. Phys., Part 2 **46**, L789 (2007).
[33] M. Suzuki and T. Uenoyama, Phys. Rev. B **52**, 8132 (1995).
[34] Within the elastic continuum model presented here it is the total width of each material that matters and not the specific sequence of layers in the multilayer system.